applied sciences

MDPI

Article

Terahertz Broadband Adjustable Absorber Based on VO_2 Multiple Ring Structure

Xiaoxin Wang [1], Guozhang Wu [2,*], Yuandong Wang [2] and Jianguo Liu [2]

[1] Beijing Space Crafts Manufacturing Co., Ltd., Beijing 100094, China
[2] State Key Laboratory on Integrated Optoelectronics, Institute of Semiconductors, Chinese Academy of Sciences, Beijing 100083, China
* Correspondence: wgzhang16@semi.ac.cn

Abstract: A broadband adjustable absorber operating in the terahertz (THz) range is presented based on a vanadium dioxide (VO_2) multiple ring structure with a certain gap design. The dynamic absorption regulation of the absorber is realized by utilizing the phase-change characteristics of VO_2, which is easily affected by external temperature. The simulation results show that when the external temperature reaches 350 K, the conductivity of VO_2 can reach 2×10^5 S/m, and the absorber can obtain an absorption efficiency of over 90% from 3.01 THz to 7.27 THz. At this time, the absorption bandwidth reaches 4.26 THz with 82.9% of the relative bandwidth. When the external temperature reaches 300 K, the conductivity changes to 200 S/m, and the absorption efficiency is less than 4%, indicating the strong THz absorption dynamic adjustable ability. Further, through analyzing the optimal impedance matching and the electric field distribution under different conductivities, the broadband absorption mechanism of the absorber can be obtained. Finally, this paper shows that the absorption spectrum cannot be influenced by small angle incidences in both polarization modes. Therefore, the ultra-wideband adjustable absorber is expected to have applications in the terahertz fields of detecting, modulating, and switching.

Keywords: terahertz; vanadium dioxide; absorber; adjustable

check for updates

Citation: Wang, X.; Wu, G.; Wang, Y.; Liu, J. Terahertz Broadband Adjustable Absorber Based on VO_2 Multiple Ring Structure. *Appl. Sci.* **2023**, *13*, 252. https://doi.org/10.3390/app13010252

Academic Editor: Roberto Zivieri

Received: 23 November 2022
Revised: 13 December 2022
Accepted: 21 December 2022
Published: 25 December 2022

Copyright: © 2022 by the authors. Licensee MDPI, Basel, Switzerland. This article is an open access article distributed under the terms and conditions of the Creative Commons Attribution (CC BY) license (https://creativecommons.org/licenses/by/4.0/).

1. Introduction

In recent years, metamaterials composed of artificial subwavelength cells have attracted extensive attention from many researchers. A great variety of functional devices stemming from metamaterials have promoted the development of electromagnetic wave control technology, because of their supernormal electromagnetic properties [1–5] that differ from natural materials [6–10]. The metamaterial absorber is an important field of metamaterial research, which can realize perfect absorption through electromagnetic resonance under the action of incident waves, causing significant energy loss. Since Landy et al. [11] first designed and validated the perfect metamaterial absorber in the microwave frequency band in 2008, the perfect metamaterial absorbers have played a significant role in the field of optics and even THz. At present, the broadband metamaterial absorber mainly realizes the superposition of multiple resonance absorption modes through the multilayer resonant structures so as to achieve broadband absorption [12–16].

The metamaterial perfect absorbers are widely used in THz applications [17–21], especially a variety of tunable metamaterial perfect absorbers based on liquid crystals, graphene, semiconductors, and phase-change materials have been shown to obtain excellent reconfigurable properties [22–38]. Among these materials, the phase-change material of VO_2 has the advantage of rapid modulation characteristics, which can achieve great transformation of conductivity at 340 K [39]. Using this characteristic of VO_2, researchers have developed broadband or even dual-band adjustable absorbers. In 2020, Jiao et al. reported a tunable dual broadband terahertz absorber based on the VO_2 structure with two groups of symmetric elliptical hollow structures, and its two bandwidths of 90% absorption were 2.32 THz

and 2.03 THz, respectively. In 2020, Huang et al. proposed a metal–dielectric-phase material tunable broadband absorber, whose top structure was made up of four identical VO_2 rectangle rings, and the absorption bandwidth reached 2.45 THz. In 2022, Yang et al. presented a broadband terahertz absorber based on a classical three-layer structure, with the absorption bandwidth up to 3.78 THz. However, although some metamaterial perfect absorbers based on VO_2 have shown broadband absorption characteristics in recent years, their bandwidth and adjustable range still need to be further expanded.

Aiming at addressing the above problems, this paper proposes a THz ultra-wideband tunable absorber based on a VO_2 multiple square ring structure, which leaves a gap with a certain thickness in the middle of the ring to enhance the resonant absorption effect. The absorption bandwidth is up to 4.26 THz, which is broader than that of other absorbers, as shown in Table 1. The absorber is not only simple and convenient for experimental preparation, but can also control its absorption intensity through temperature regulation. It has a broadband absorption bandwidth in the metal phase of VO_2, and has polarization and incidence-insensitive absorption properties.

Table 1. Comparison of absorption performance of other absorbers with that of the absorber proposed in this paper.

Reference	Material	Bandwidth (Absorptance over 90%) (THz)	Relative Bandwidth (%)	Tunable Range (%)
[32]	VO_2	0.99 − 0.47 = 0.52	71.2	5–100
[33]	VO_2	5.57 − 4.32 = 1.25	25.3	15–96
[34]	VO_2 and graphene	3.21 − 1.69 = 1.52	62.0	22.6–99.2
[35]	VO_2 and graphene	3.08 − 1.29 = 1.79	81.9	20–99
[36]	VO_2	4.19 − 1.87 = 2.32 10.73 − 8.70 = 2.03	76.6 20.9	2–94
[37]	VO_2	4.30 − 1.85 = 2.45	79.7	4–100
[38]	VO_2	6.79 − 3.01 = 3.78	77.1	2.7–98.9
This paper	VO_2	7.27 − 3.01 = 4.26	82.9	4–100

2. Structure Design and Simulation

The broadband adjustable absorber adopts a sandwich structure based on a VO_2 multiple ring structure, which is shown in Figure 1. The bottom metal structure applies gold as the reflect layer, and SiO_2 (a dielectric constant of 3.8) as the dielectric layer. The top layer employs the phase-change material VO_2, which consists of two square ring structures L_1 and L_2 with different sizes and a patch structure L_3. It is worth noting that a gap with a certain thickness of 0.08 μm is left in the middle to enhance the resonance absorption effect. The optimized structural parameters are as follows: the cell period p = 24 μm, the bottom layer thickness h_1 = 0.2 μm, the medium layer height d = 7 μm, and the top layer thickness of the VO_2 h_2 = 0.2 μm. The dimensions of the ring structure and patch structure are followed by l_1 = 20 μm, l_2 = 12 μm, and l_3 = 4 μm, with a width of w = 2 μm. In the THz range, the optical characteristics of VO_2 can be described through the Drude model [40,41], as shown in Formula (1):

$$\varepsilon(\omega) = \varepsilon_\infty - \frac{\omega_p^2}{(\omega^2 + i\gamma\omega)} \quad (1)$$

where the high-frequency dielectric constant ε_∞ and the collision frequency γ are 12 and 5.75×10^{13} rad/s, respectively. What is more, the plasma frequency ω_p can be expressed by Formula (2):

$$\omega_p^2 = \frac{\sigma}{\sigma_0}\omega_p^2(\sigma_0) \quad (2)$$

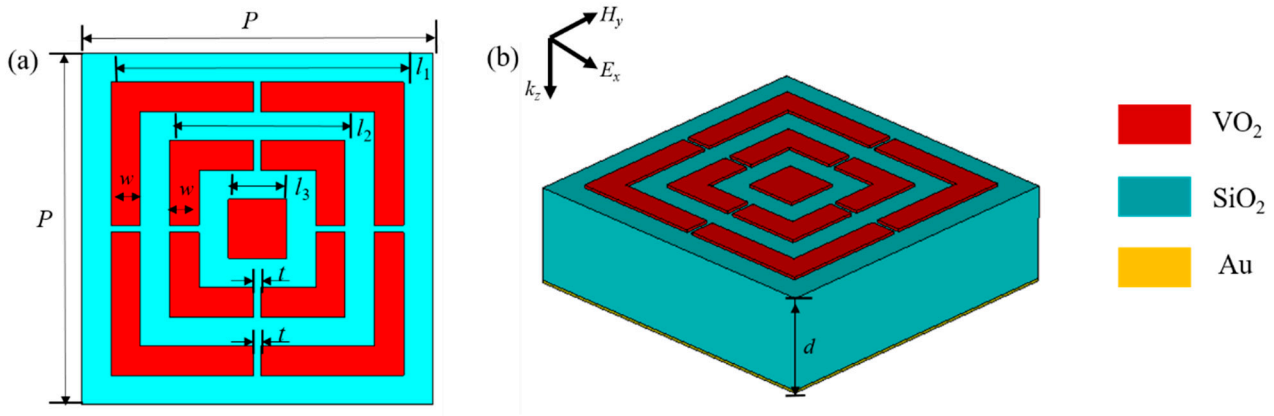

Figure 1. Unit cell of the structure in (**a**) top view and (**b**) three-dimensional schematic.

The conductivity σ_0 in Formula (2) is 3×10^5 S/m and $\omega_p(\sigma_0)$ is 1.4×10^{15} rad/s. We mainly study the influence of conductivity caused by the temperature change of VO_2 from the insulation phase to the metal phase on the absorption performance [42]. Here, the conductivity of VO_2 is 200 S/m when the external temperature is 300 K, and changes dramatically to 2×10^5 S/m when the external temperature is 350 K. Then, the finite element method with periodic boundary conditions (PBC) is set in the X and Y directions to simulate Figure 1b. The electromagnetic wave is perpendicular to the surface of the structure along the negative Z direction. The conductivity of Au is 4.56×10^7 S/m and the thickness is more than the skin depth of THz. Thus, the transmission of THz can be ignored so that the transmittance of the electromagnetic wave after the incident is equivalent to zero. Then, the absorption performance of the electromagnetic wave can be expressed as Formula (3):

$$A(\omega) = 1 - R(\omega) = 1 - |S_{11}(\omega)|^2 \quad (3)$$

where $R(\omega)$ and $S_{11}(\omega)$ are the reflectivity and the reflection coefficient from the frequency-dependent S parameter.

3. Simulation Results

Firstly, the Figure 2a exhibits the best absorption state of the absorber when the conductivity of VO_2 is 2×10^5 S/m. It can be seen from the result that under the condition of vertical incidence, the bandwidth greater than 90% absorption efficiency is as high as 4.26 THz and the frequency covers 3.01 THz to 7.27 THz. To verify the effect of polarization on the incident electromagnetic wave, the absorptivity under different polarization angles is simulated in Figure 2b. The absorption performance of the absorber remains consistent and confirms that the absorber is hardly affected by the polarization angle.

Next, the absorption and reflection spectrum can change dynamically accordingly to the conductivity variety of VO_2. In Figure 3, when the conductivities of VO_2 change from 200 S/m to 2×10^5 S/m, the absorption and reflection rate varies between 4% and 100%. At this time, the central frequency of the spectrum remains almost invariant at 5.17 THz, but the absorption peak has changed from the single absorption peak to double absorption peaks, with the increasing absorption bandwidth. The variety of the dielectric constant of VO_2, which affects the overall absorption efficiency with the change of conductivities, can be taken into consideration to explain this phenomenon. It can be seen from Figure 4 that the imaginary part of the dielectric constant is much greater than the real part, which is the main factor of the absorption effect. With the increase in the conductivities, the imaginary part arises rapidly, thereby improving the overall absorption efficiency of the absorber. The results show that when the conductivities of VO_2 are actively controlled by temperature, the absorber has tunable absorption characteristics. In addition, the properties of VO_2 can also be adjusted by electricity [43] or heat [39] to realize the dynamic tuning of the working bandwidth and absorption efficiency.

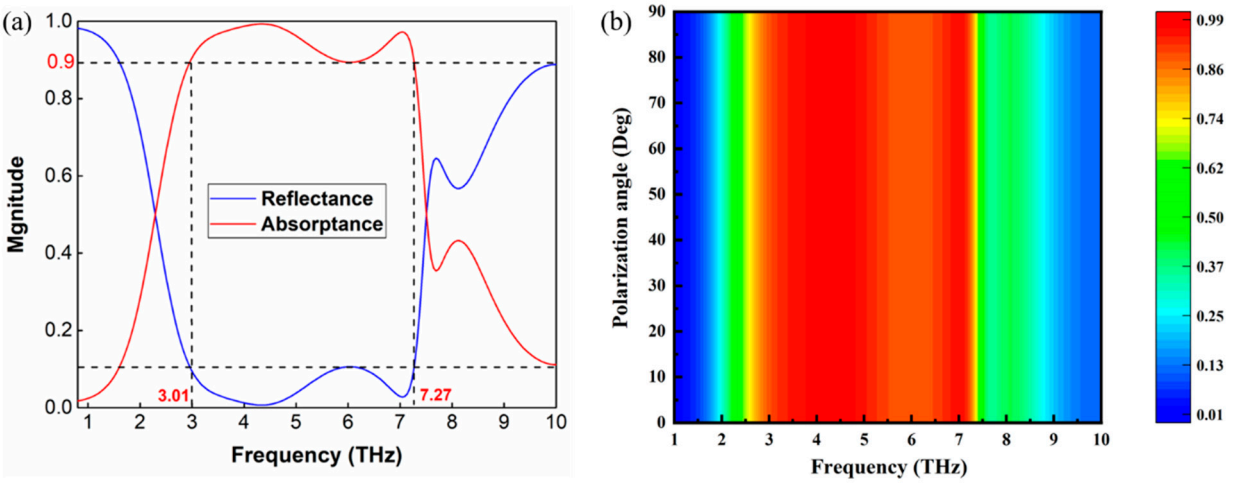

Figure 2. (**a**) Optimal absorption and reflection spectrum and (**b**) absorption spectrum at different polarization angles when $\sigma = 2 \times 10^5$ S/m.

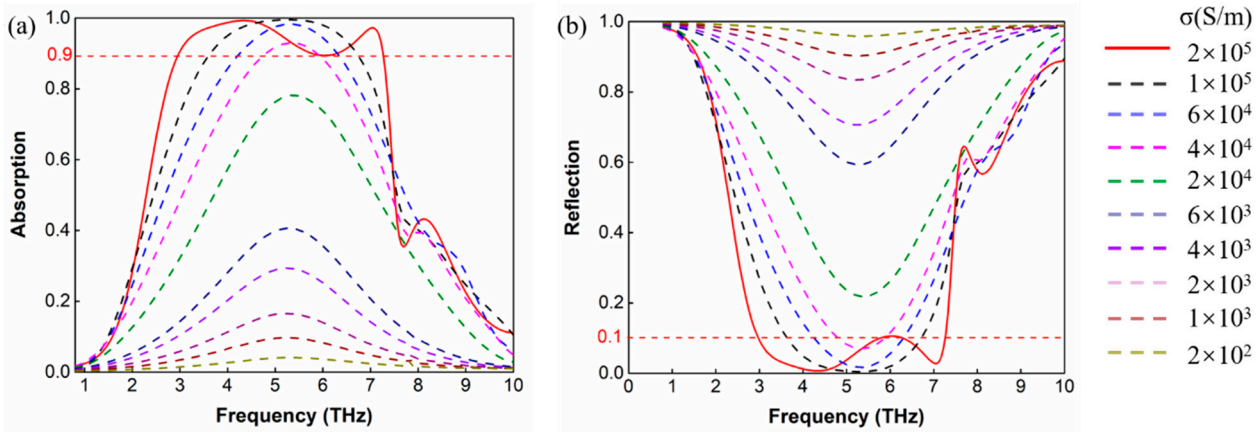

Figure 3. (**a**) Absorption spectrum and (**b**) reflection spectrum of absorber under different conductivities of VO_2.

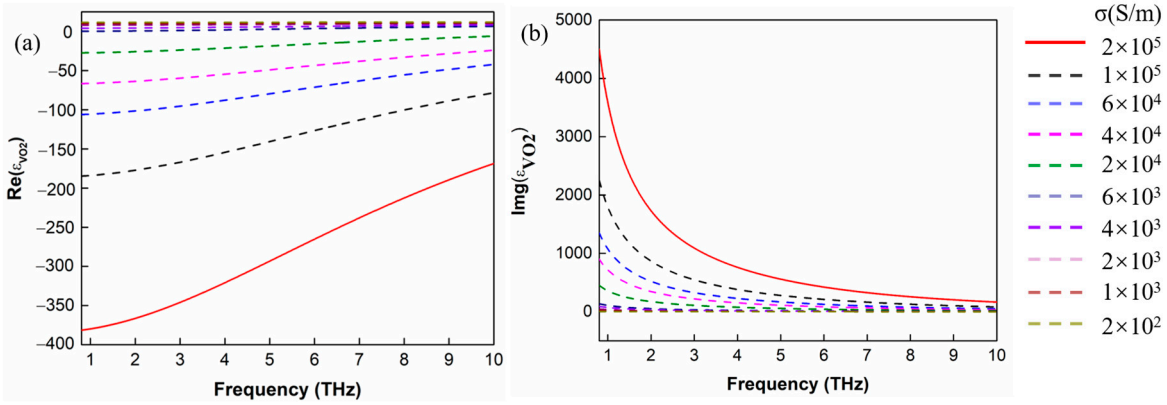

Figure 4. Change of dielectric constant of VO_2 under different conductivities in (**a**) the real part and (**b**) the imaginary part.

4. Discussion

To explain the adjustable principle, the electric field distribution at the center frequency of 5.17 THz is studied at a variety of conductivities from 2×10^2 S/m to 2×10^5 S/m in Figure 5. The results show that the electric field distribution is very weak and nearly negligible at a conductivity of 2×10^2 S/m in Figure 5a. When the conductivity is increased

to 2×10^5 S/m, the electric field intensity is greatly strengthened because the resonance absorption effect of the gaps is improved, thereby enhancing the overall absorption effect in Figure 5d. Therefore, the dynamic function of the absorber can be achieved by regulating the conductivity of VO_2. In the meantime, when VO_2 stands in the metal phase, the corresponding impedance of the absorber matches that of the vacuum. Here, the relative impedance Z_r is given when the conductivity of VO_2 is 2×10^5 S/m, as in Figure 6. The value of the impedance of free space Z_0 is equal to 1, and that of the absorber is Z, which is expressed by Formula (4) [44]:

$$Z = \frac{\mu(\omega)}{\varepsilon(\omega)} = \sqrt{\frac{(1+S_{11})^2 - S_{21}^2}{(1-S_{11})^2 - S_{21}^2}}, Z_r = \frac{Z}{Z_0} \quad (4)$$

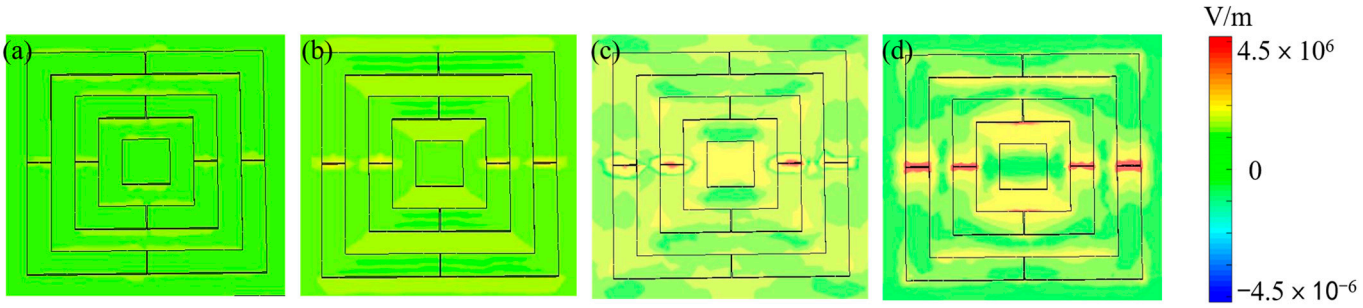

Figure 5. Electric field distribution at the center frequency of 5.17 THz when the conductivity of VO_2 is (**a**) 2×10^2 S/m, (**b**) 2×10^3 S/m, (**c**) 2×10^4 S/m, and (**d**) 2×10^5 S/m.

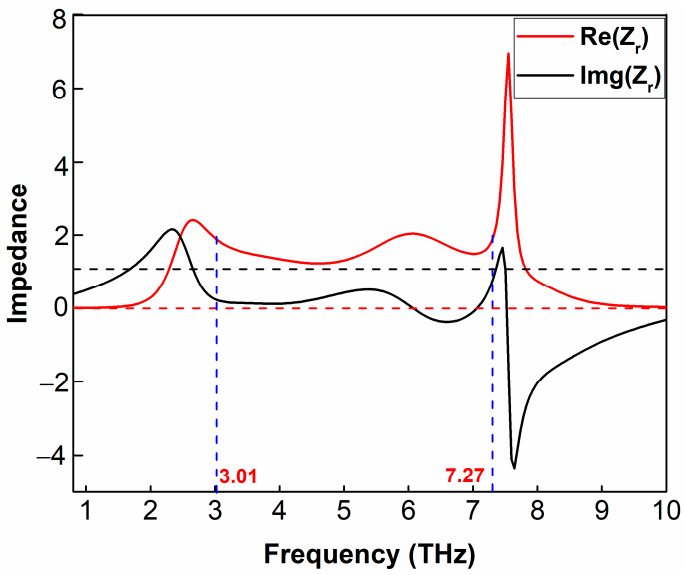

Figure 6. Relative impedance Z_r diagram of the absorber at a conductivity of 2×10^5 S/m.

The S_{11} and S_{21} are the reflection and transmission coefficient of the S-parameter, respectively. When Z is equal to Z_0, the surface reflection of the absorber reaches zero, indicating the attainment of the impedance matching. The figure reveals that the real part and imaginary part of the relative impedance are approximate to 1 and zero from 3.01 THz to 7.27 THz, explaining that the impedance between the absorber and free space is almost consistent, which conforms to the perfect absorption mechanism. Thus, the perfect absorption mechanism can be well illuminated through the impedance-matching theory.

It is also important to analyze the effect of the geometric structure of the designed absorber on the absorption spectrum from optimizing the key parameters. Here, the VO_2 and SiO_2 with different thicknesses are applied to sweep the parameters of the top and

middle layers in Figure 7. In Figure 7a, the absorption intensity first arises along with the addition of the top layer thickness, and then decreases with the further increase beyond the optimal value. Obviously, the absorption of the absorber is easily affected by the thickness of VO_2. The coupling effect of VO_2 with the bottom metal is very weak when its thickness is very thin. However, when its thickness turns thick enough, it exhibits a strong reflection effect, which is not conducive to matching the impedance of the vacuum. The optimal thickness of VO_2 is 0.2 μm, and the broadband absorption range over than 90% absorptivity varies from 3.01 THz to 7.27 THz. In addition, the absorption spectrum affected by the dielectric thickness is also discussed in Figure 7b. Firstly, the central frequency of the spectrum is 5.17 THz, corresponding to the free space wavelength of 58 μm. Next, the refractive index of SiO_2 is n = 1.95 ($3.8^{0.5}$), so that the corresponding central wavelength equals 29 μm in the dielectric layer. Here, the optimal thickness of the middle layer is 7 μm, which is almost equivalent to one fourth of the central frequency, and meets the interference cancellation effect between the reflected waves and incident waves. Thus, the perfect absorption mechanism can also be explained by the wave-interference cancellation theory. As a result, it is meaningful to study the thickness of VO_2 and SiO_2 for their improvements to the absorption performance.

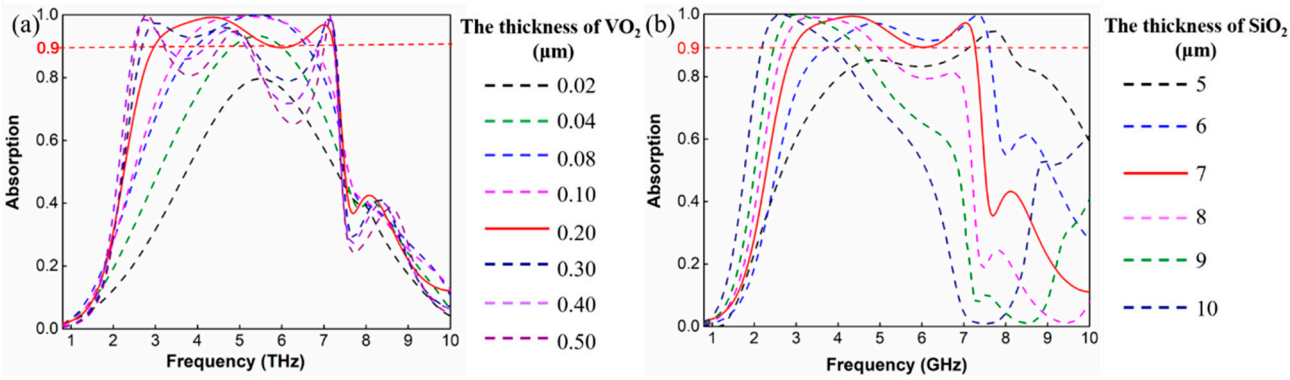

Figure 7. Absorption spectrum of different thicknesses of (**a**) VO_2 and (**b**) SiO_2 when σ equals 2×10^5 S/m.

Figure 8 presents the absorption performance of the different geometric parameters of VO_2. The different ring lengths will affect the coupling between the rings, so the optimal ring sizes l_1, l_2, and l_3 can be obtained by scanning different sizes. As a result, the optimal structure parameters include l_1 = 20 μm, l_2 = 12 μm, l_3 = 4 μm, w = 2 μm, and t = 0.08 μm. In Figure 8d, when the ring width increases, the number of absorption peaks in the absorption spectrum will change from one to two and the overall absorption bandwidth will also change greatly. Similarly, the gap width t on the rings will affect the overall absorption bandwidth and efficiency significantly, as in Figure 8e. The value t = 0.08 μm is the most ideal result of the gap width in the proposed design. It is worth noting that the complete structure shows greater absorption bandwidth and efficiency than a single ring with and without a gap, indicating that the integration of different structures adds to the resonance absorption of different frequencies, as in Figure 8f. Moreover, the increase in the number of rings helps to improve the overall absorption bandwidth and efficiency because the absorption performance of double rings is better than a single ring (Figure 8f). The optimal number of rings can be obtained by simulating the absorption efficiency of the multi-ring structure.

Finally, the above discussions mainly focus on the case of vertical incidence; thus, the influence of oblique incidence on the absorption will be further illuminated in this part. To analyze whether the absorber possesses a good absorption performance or not under oblique incidence, the absorption effect at different angles is simulated through the full wave simulation in Figure 9, including transverse electric polarization (TE) and transverse magnetic polarization (TM). Figure 9a shows that for the TE polarized waves, the absorption

spectrum will not change at small angles (up to 55°), and its absorptivity will remain above 75% between 3.01 THz and 7.27 THz. For the TM polarized waves in Figure 9b, the main absorption peak in the spectrum narrows slightly along with increasing the incident angles. The absorption bandwidth narrows and higher-order modes appear as the incident angle reaches 25°. At the same time, the ratio of the wavelength (58 µm, 5.17 THz) and period (24 µm) is 2.42, which cannot meet the demand of the sub-wavelength scale for large angle incidence, so it tends to have some grating lobes and high-order diffraction. Thus, the above results show that the absorber works well at small incident angles.

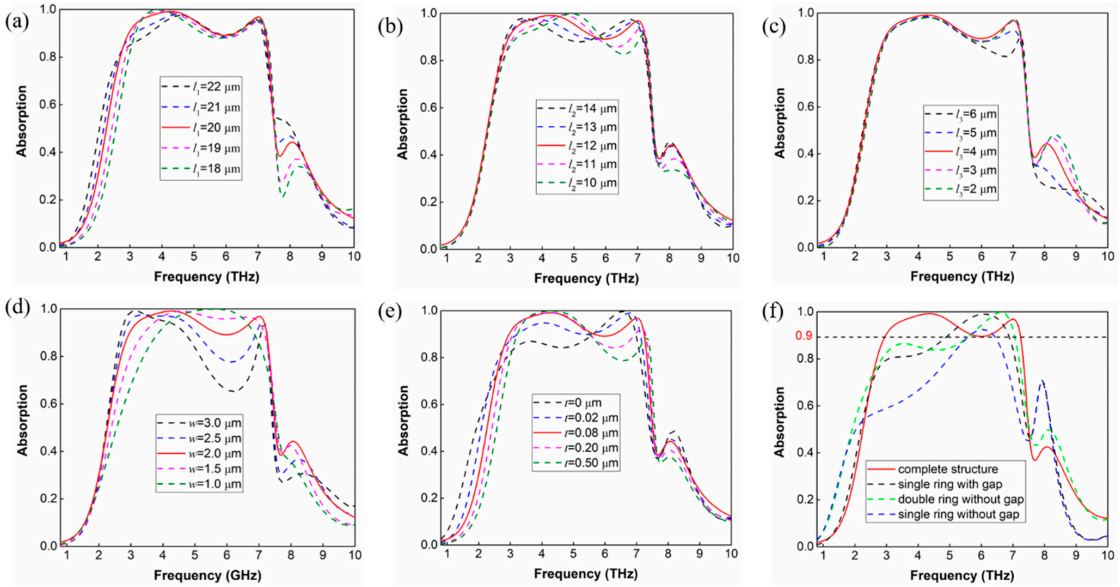

Figure 8. Absorption spectrum of different geometric parameters such as (**a**) the length of outer ring l_1, (**b**) the length of middle ring l_2, (**c**) the length of inter block l_3, (**d**) the width of rings w, (**e**) the gap width t on the rings, and (**f**) four different structures.

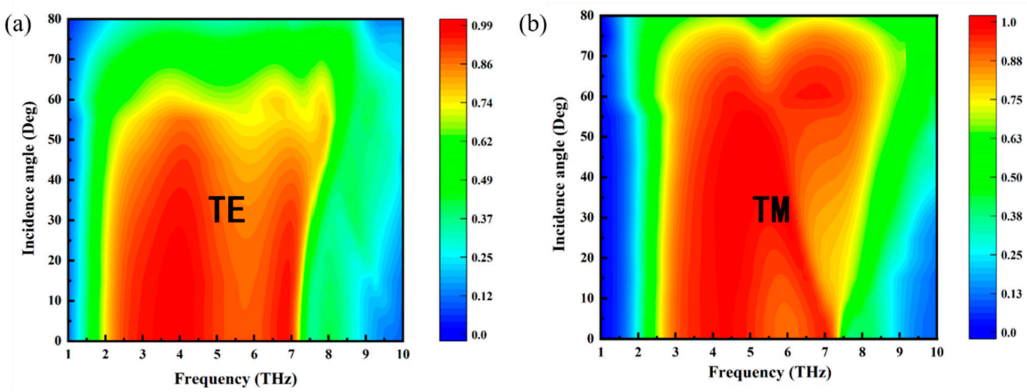

Figure 9. Absorption spectrum at oblique incident under different polarizations. (**a**) TE mode and (**b**) TM mode.

5. Conclusions

A THz ultra-wideband tunable absorber is proposed based on the multiple ring structure of the phase-change material VO_2. By using the phase-change characteristics of VO_2 affected by temperature, the absorber can not only regulate the absorption efficiency, but also control the absorption bandwidth. The simulation results show that when the conductivities of VO_2 is affected by an external temperature change from 200 S/m to 2×10^5 S/m, the absorption rate varies from 4% to 100%. The optimal absorption bandwidth of the absorber reaches 4.26 THz, with the relative bandwidth of 82.9%, which is better than that of the absorbers mentioned in Table 1. The optimal impedance-matching analysis and the

different electric field distribution under different conductivities of VO_2 can qualitatively explicate the broadband absorption mechanism. In the meantime, we can quantitatively study the absorption principle by employing the wave-interference cancellation theory from analyzing the influence of the top two layers' thickness. Finally, by analyzing the influence of oblique incidence on the absorptivity, this paper shows that the designed absorber is little affected by small incident angles. Therefore, the research has certain guiding significance for the application of tunable absorbers in the fields of detection, modulation, and switching.

Author Contributions: Conceptualization, X.W.; methodology, X.W.; formal analysis, X.W.; investigation, X.W.; data curation, X.W. and G.W.; writing—original draft preparation, X.W. and G.W.; writing—review and editing, X.W., G.W. and Y.W.; supervision, J.L. and G.W.; funding acquisition, J.L. All authors have read and agreed to the published version of the manuscript.

Funding: This research was supported by the National Key Research and Development Program of China (No. 2019YFB2203700 and No. 2018YFB2200500), and Natural Science Foundation of Shandong Province (No. ZR2020MF106).

Institutional Review Board Statement: Not applicable.

Informed Consent Statement: Not applicable.

Data Availability Statement: Not applicable.

Conflicts of Interest: The authors declare no conflict of interest.

References

1. Shelby, R.A.; Smith, D.R.; Schultz, S. Experimental verification of a negative index of refraction. *Science* **2001**, *292*, 77–79. [CrossRef] [PubMed]
2. Diincer, F.; Sabah, C.; Karaaslan, M.; Unal, E.; Bakir, M.; Erdiven, U. Asymmetric transmission of linearly polarized waves and dynamically wave rotation using chiral metamaterial. *Prog. Electromagn. Res.* **2013**, *140*, 227–239. [CrossRef]
3. Diincer, F.; Karaaslan, M.; Akgol, O.; Unal, E.; Sabah, C. Asymmetric transmission of linearly polarized electromagnetic waves using chiral metamaterials with constant chirality over a certain frequency band. *Mode. Phys. Lett. B* **2014**, *28*, 1450250. [CrossRef]
4. Bae, M.H.; Oh, J.H. Nonlinear elastic metamaterial for tunable bandgap at quasi-static frequency. *Mech. Syst. Signal Process.* **2022**, *170*, 108832. [CrossRef]
5. Li, C.Q.; Song, Z.Y. Tailoring terahertz wavefront with state switching in VO_2 Pancharatnam–Berry metasurfaces. *Opt. Laser Technol.* **2023**, *157*, 108764. [CrossRef]
6. Li, J.P.; Jin, R.H.; Geng, J.P.; Liang, X.L.; Wang, K.; Premaratne, M.; Zhu, W.R. Design of a broadband metasurface luneburg lens for full-angle operation. *IEEE Trans. Antennas. Propag.* **2019**, *67*, 2442–2451. [CrossRef]
7. Cummer, S.A.; Popa, B.I.; Schurig, D.; Smith, D.R.; Pendry, J. Full-wave simulations of electromagnetic cloaking structures. *Phys. Rev. E* **2006**, *74*, 036621. [CrossRef]
8. Cai, W.S.; Chettiar, U.K.; Kildishev, A.V.; Shalaev, V.M. Optical cloaking with metamaterials. *Nat. Photonics* **2007**, *1*, 224–227. [CrossRef]
9. Kwon, D.H.; Werner, P.L.; Werner, D.H. Optical planar chiral metamaterial designs for strong circular dichroism and polarization rotation. *Opt. Express* **2008**, *16*, 11802–11807. [CrossRef]
10. Almoneef, T.S.; Ramahi, M. Metamaterial electromagnetic energy harvester with near unity efficiency. *Appl. Phys. Lett.* **2015**, *106*, 153902. [CrossRef]
11. Landy, N.I.; Sajuyigbe, S.; Mock, J.J.; Smith, D.R.; Padilla, W.J. Perfect metamaterial absorber. *Phys. Rev. Lett.* **2008**, *100*, 207402. [CrossRef] [PubMed]
12. Shen, N.H.; Massaouti, M.; Gokkavas, M.; Manceau, J.M.; Ozbay, E.; Kafesaki, M.; Koschny, T.; Tzortzakis, S.; Soukoulis, C.M. Optically implemented broadband blueshift switch in the terahertz regime. *Phys. Rev. Lett.* **2011**, *106*, 037403. [CrossRef] [PubMed]
13. Wang, B.X.; Wang, G.Z. Temperature tunable metamaterial absorber at THz frequencies. *J. Mater. Sci.-Mater. Electron.* **2017**, *28*, 8487–8493. [CrossRef]
14. Zhang, Y.P.; Li, Y.; Cao, Y.Y.; Liu, Y.Z.; Zhang, H.Y. Graphene induced tunable and polarization-insensitive broadband metamaterial absorber. *Opt. Commun.* **2017**, *382*, 281–287. [CrossRef]
15. Pan, W.; Yu, X.; Zhang, J.; Zeng, W. A novel design of broadband terahertz metamaterial absorber based on nested circle rings. *IEEE Photon. Technol. Lett.* **2016**, *28*, 2335–2338. [CrossRef]
16. Rahmanzadeh, M.; Rajabalipanah, H.; Abdolali, A. Multilayer graphene-based metasurfaces: Robust design method for extremely broadband, wide-angle, and polarization-insensitive terahertz absorbers. *Appl. Opt.* **2018**, *57*, 959–968. [CrossRef]
17. Campbell, S.D.; Grobe, S.D.; Goodin, I.L.; Su, Q.; Grobe, R. Limitations of decomposition-based imaging of longitudinal absorber configurations. *Phys. Rev. A* **2008**, *77*, 023821. [CrossRef]

18. Chen, H.; Ma, W.; Huang, Z.; Zhang, Y.; Huang, Y.; Chen, Y. Graphene-Based Materials toward Microwave and THz Absorbing Stealth Technologies. *Adv. Opt. Mater.* **2019**, *7*, 1801318. [CrossRef]
19. Karthikeyan, M.; Jayabala, P.; Ramachandran, S.; Dhanabalan, S.S.; Sivanesan, T.; Ponnusamy, M. Tunable Optimal Dual Band Metamaterial Absorber for High Sensitivity THz Refractive Index Sensing. *Nanomaterials* **2022**, *15*, 2693. [CrossRef]
20. Li, Z.R.; Cheng, Y.Z.; Luo, H.; Chen, F.; Li, X.C. Dual-band tunable terahertz perfect absorber based on all-dielectric InSb resonator structure for sensing application. *J. Alloys Compd.* **2022**, *925*, 166617. [CrossRef]
21. Liu, W.W.; Song, Z.Y. Terahertz absorption modulator with largely tunable bandwidth and intensity. *Carbon* **2022**, *174*, 617–624. [CrossRef]
22. Wen, Q.Y.; Zhang, H.W.; Yang, Q.H.; Chen, Z.; Long, Y.; Jing, Y.L.; Lin, Y.; Zhang, P.X. A tunable hybrid metamaterial absorber based on vanadium oxide films. *J. Phys. D Appl. Phys.* **2012**, *45*, 235106. [CrossRef]
23. Deng, H.; Stan, L.; Czaplewski, D.A.; Gao, J.; Yang, X. Broadband infrared absorbers with stacked double chromium ring resonators. *Opt. Express* **2017**, *25*, 28295–28304. [CrossRef]
24. Hao, J.P.; Lheurette, E.; Burgnies, L.; Okada, E.; Lippens, D. Bandwidth enhancement in disordered metamaterial absorbers. *Appl. Phys. Lett.* **2014**, *105*, 081102. [CrossRef]
25. Chen, L.; Song, Z. Simultaneous realizations of absorber and transparent conducting metal in a single metamaterial. *Opt. Express* **2020**, *28*, 6565–6571. [CrossRef]
26. Song, Z.; Zhang, J. Achieving broadband absorption and polarization conversion with a vanadium dioxide metasurface in the same THz frequencies. *Opt. Express* **2020**, *28*, 12487–12497. [CrossRef]
27. Cheng, Y.; Gong, R.; Cheng, Z. A photoexcited broadband switchable metamaterial absorber with polarization-insensitive and wide-angle absorption for THz waves. *Opt. Commun.* **2016**, *361*, 41–46. [CrossRef]
28. Wang, R.; Li, L.; Liu, J.; Yan, F.; Tian, F.; Tian, H.; Zhang, J.; Sun, W. Triple-band tunable perfect THz metamaterial absorber with liquid crystal. *Opt. Express* **2017**, *25*, 32280–32289. [CrossRef]
29. Li, J.S.; Yan, D.X.; Sun, J.Z. Flexible dual-band all-graphene-dielectric THz absorber. *Opt. Mater. Express* **2019**, *9*, 2067–2075. [CrossRef]
30. Liu, L.; Liu, W.; Song, Z. Ultra-broadband THz absorber based on a multilayer graphene metamaterial. *J. Appl. Phys.* **2020**, *128*, 093104. [CrossRef]
31. Jiang, M.; Song, Z.; Liu, Q. Ultra-broadband wide-angle THz absorber realized by a doped silicon metamaterial. *Opt. Commun.* **2020**, *471*, 125835. [CrossRef]
32. Song, Z.; Wei, M.; Wang, Z.; Cai, G.; Liu, Y.; Zhou, Y. Terahertz absorber with reconfigurable bandwidth based on isotropic vanadium dioxide metasurfaces. *IEEE Photon. J.* **2019**, *11*, 4600607. [CrossRef]
33. Bai, J.; Zhang, S.; Fan, F.; Wang, S.; Sun, X.; Miao, Y.; Chang, S. Tunable broadband THz absorber using vanadium dioxide metamaterials. *Opt. Commun.* **2019**, *452*, 292–295. [CrossRef]
34. Li, H.; Yu, J.; Chen, Z. Broadband Tunable Terahertz Absorber Based on Hybrid Graphene-Vanadium Dioxide Metamaterials. *Chin. J. Lasers* **2020**, *47*, 0903001. [CrossRef]
35. Zhou, Z.; Song, Z. Switchable bifunctional metamaterial for terahertz anomalous reflection and broadband absorption. *Phys. Scr.* **2021**, *96*, 115506. [CrossRef]
36. Jiao, X.F.; Zhang, Z.H.; Li, T.; Xu, Y.; Song, G.F. Tunable Dual Broadband Terahertz Metamaterial Absorber Based on Vanadium Dioxide. *Appl. Sci.* **2020**, *10*, 7259. [CrossRef]
37. Huang, J.; Li, J.; Yang, Y.; Li, J.; Li, J.; Zhang, Y.; Yao, J. Broadband terahertz absorber with a flexible, reconfigurable performance based on hybrid-patterned vanadium dioxide metasurfaces. *Opt. Express* **2020**, *28*, 17832–17840. [CrossRef]
38. Yang, G.; Yan, F.; Du, X.; Li, T.; Wang, W.; Lv, Y.; Zhou, H.; Hou, Y. Tunable broadband terahertz metamaterial absorber based on vanadium dioxide. *AIP Adv.* **2022**, *12*, 045219. [CrossRef]
39. Wen, Q.Y.; Zhang, H.W.; Yang, Q.H.; Xie, Y.S.; Chen, K.; Liu, Y.L. THz metamaterials with VO2 cut-wires for thermal tunability. *Appl. Phys. Lett.* **2010**, *97*, 021111. [CrossRef]
40. Liu, M.; Hwang, H.Y.; Tao, H.; Strikwerda, A.C.; Fan, K.; Keiser, G.R.; Sternbach, A.J.; West, K.G.; Kittiwatanakul, S.; Lu, J.; et al. THz-field-induced insulator-to-metal transition in vanadium dioxide metamaterial. *Nature* **2012**, *487*, 345–348. [CrossRef]
41. Wang, S.; Kang, L.; Werner, D.H. Hybrid resonators and highly tunable terahertz metamaterials enabled by vanadium dioxide (VO2). *Sci. Rep.* **2017**, *7*, 4326. [CrossRef] [PubMed]
42. Liu, H.; Wong, L.; Wang, S.; Tang, S.; Zhang, X. Ultrafast insulator–metal phase transition in vanadium dioxide studied using optical pump–THz probe spectroscopy. *J. Phys. Condens. Matter* **2012**, *24*, 415604. [CrossRef] [PubMed]
43. Liu, L.; Kang, L.; Mayer, T.S.; Werner, D.H. Hybrid metamaterials for electrically triggered multifunctional control. *Nat. Commun.* **2016**, *7*, 13236. [CrossRef] [PubMed]
44. Smith, D.R.; Schultz, S.; Markoš, P.; Soukoulis, C.M. Determination of effective permittivity and permeability of metamaterials from reflection and transmission coefficients. *Phys. Rev. B* **2002**, *65*, 195104. [CrossRef]

Disclaimer/Publisher's Note: The statements, opinions and data contained in all publications are solely those of the individual author(s) and contributor(s) and not of MDPI and/or the editor(s). MDPI and/or the editor(s) disclaim responsibility for any injury to people or property resulting from any ideas, methods, instructions or products referred to in the content.